Longer time steps for molecular dynamics

Jesús A. Izaguirre[a)]
Beckman Institute and Department of Computer Science, University of Illinois at Urbana-Champaign, Urbana, Illinois 61801

Sebastian Reich
Department of Mathematics and Statistics, University of Surrey, Guildford GU3 5XH, United Kingdom

Robert D. Skeel
Beckman Institute and Department of Computer Science, University of Illinois at Urbana-Champaign, Urbana, Illinois 61801

(Received 24 August 1998; accepted 3 March 1999)

Simulations of the dynamics of biomolecules have been greatly accelerated by the use of multiple time-stepping methods, such as the Verlet-I/r-RESPA (reversible reference system propagator algorithms) method, which is based on approximating ''slow'' forces as widely separated impulses. Indeed, numerical experiments have shown that time steps of 4 fs are possible for these slow forces but unfortunately have also shown that a long time step of 5 fs results in a dramatic energy drift. To overcome this instability, a symplectic modification of the impulsive Verlet-I/r-RESPA method has been proposed, called the mollified impulse method. The idea is that one modifies the slow part of the potential energy so that it is evaluated at ''time averaged'' values of the positions, and one uses the gradient of this modified potential for the slow part of the force. By filtering out excitations to the fastest motions, these averagings allow the use of longer time steps than does the impulse method. We introduce a new mollified method, *Equilibrium*, that avoids instability in a more effective manner than previous averaging mollified methods. Our experiments show that *Equilibrium* with a time step of 6 fs is as stable as the impulsive Verlet-I/r-RESPA method with a time step of 4 fs. We show that it may be necessary to include the effect of nonbonded forces in the averaging to make yet longer time steps possible. We also show that the slight modification of the potential has little effect on accuracy. For this purpose we compare self-diffusion coefficients and radial distribution functions against the Leapfrog method with a short time step (0.5 fs). © *1999 American Institute of Physics.* [S0021-9606(99)01520-2]

I. INTRODUCTION

Simulations of the dynamics of biomolecules have been greatly accelerated by the use of multiple time-stepping methods, such as the Verlet-I/r-RESPA method, which is based on approximating ''slow'' forces as widely separated impulses. (This method was proposed but not implemented by the authors of Refs. 1 and 2, and independently discovered by the authors of Ref. 3, who also demonstrated its usefulness.) Indeed, numerical experiments have shown that time steps of 4 fs are possible for these slow forces, but unfortunately have also shown that a long time step of 5 fs results in a dramatic energy drift. To overcome this instability, a modification of the impulsive Verlet-I/r-RESPA method has been proposed, called the mollified impulse method (MOLLY),[4] which allows the use of longer time steps.[5] We introduce a new *Equilibrium* version of MOLLY that avoids instability in a more effective manner than previous averaging mollified methods. Our experiments show that *Equilibrium* with a time step of 6 fs is as stable as the impulsive Verlet-I/r-RESPA method with a time step of 4 fs. We also compare dynamical and structural properties (self-diffusion coefficient and radial distribution functions) against the leapfrog method with a short time step (0.5 fs).

Molecular dynamics (MD) is a well-established technique in biophysical simulations.[6] The central question answered in this area is the relationship among structural and functional properties of proteins with respect to atomic interactions. MD requires the solution of Newton's equations of motion for a classical unconstrained simulation

$$M\frac{\mathrm{d}^2}{\mathrm{d}t^2}X(t) = -\nabla U(X(t)), \tag{1}$$

where M is a diagonal matrix of atomic masses, $x = X(t)$ are the atomic trajectories, and the potential field U is typically given by

$$U = U^{\mathrm{bnd}} + U^{\mathrm{nonbnd}}, \tag{2}$$

$$U^{\mathrm{bnd}} = U^{\mathrm{bond}} + U^{\mathrm{angle}} + U^{\mathrm{dihedral}} + U^{\mathrm{improper}}, \tag{3}$$

$$U^{\mathrm{nonbnd}} = U^{\mathrm{Lennard\text{-}Jones}} + U^{\mathrm{electrostatic}}. \tag{4}$$

The dynamics of such a system can be described, as a first approximation, as a superposition of harmonic oscillations called *normal modes* whose frequencies are obtained by performing normal mode analysis (NMA). This analysis of biological systems reveals that normal mode motions occur in disparate time scales. Bonded forces in Eq. (2) correspond to very high-frequency motions, whereas nonbonded forces have mostly low-frequency motions (see Sec. IV B).

a)Electronic mail: izaguirr@uiuc.edu

When these systems of ordinary differential equations are numerically integrated, the fastest motions restrict the time step. For the popular Verlet or leapfrog integrators, this is typically 1 fs. The real problem is that the computation of the (slower motion) nonbonded forces accounts for most of the computational time, since there are many more of these forces. To alleviate this computation burden imposed by the small time-step restriction, simulations are sometimes done with a cutoff in the nonbonded forces. However, there is increasing evidence that this introduces serious artifacts into the simulations.[2,7,8] Situations where it is especially important to include full electrostatics are: (a) When simulating charged species such as molten salts;[6] (b) when computing properties such as the dielectric constant; (c) whenever DNA is involved in the simulation.[9] The development of multiple time stepping methods has facilitated the inclusion of full electrostatics. These methods integrate different components of the force field using different time steps, and therefore are well suited to the nature of the systems. Hence, slow (long-ranged) forces are sampled less frequently than ''fast'' (short-ranged) forces.

A. Verlet-I/r-RESPA multiple time stepping (MTS)

A method that integrates different force terms using different time steps is the Verlet-I/r-RESPA impulse MTS method. We start by rewriting Eq. (1) as

$$M\frac{\mathrm{d}^2}{\mathrm{d}t^2}X = F^{\mathrm{fast}}(X) + F^{\mathrm{slow}}(X), \tag{5}$$

where $F^{\mathrm{fast}} = -U_x^{\mathrm{fast}}$ and $F^{\mathrm{slow}} = -U_x^{\mathrm{slow}}$. The partitioning of F into F^{fast} and F^{slow} is chosen so that an appropriate time step Δt for the slow part is larger than a time step δt for the fast part. As an illustration, the electrostatic force could be split into a fast and slow part as shown in Fig. 1.

With these definitions in place, the impulse method is

$$M\frac{\mathrm{d}^2}{\mathrm{d}t^2}X = \sum_{m=-\infty}^{\infty} \delta t\,\boldsymbol{\delta}(t - m\,\delta t)F^{\mathrm{fast}}(X) + \sum_{n=-\infty}^{\infty} \Delta t\,\boldsymbol{\delta}(t - n\Delta t)F^{\mathrm{slow}}(X). \tag{6}$$

Trains of impulses at different frequencies sample different force components, as illustrated in Fig. 2. Although unconstrained dynamics is being considered here, the ideas extend to the case where bond lengths (and bond angles) are constrained. In fact, results for the Verlet-I/r-RESPA method using constrained dynamics are reported in Sec. III C. Results using this approach have been reported in Refs. 10–12.

B. Symplectic and reversible integrators

An important property of the Verlet-I/r-RESPA impulse MTS method is that it is symplectic.[13] Here, we explain its significance. Numerical integrators for MD need to produce correct results for long integration periods, since simulations of tens of thousands of atoms for one or more nanoseconds are often necessary. Therefore, it is important to assess the validity of the numerical integration after such a long time.

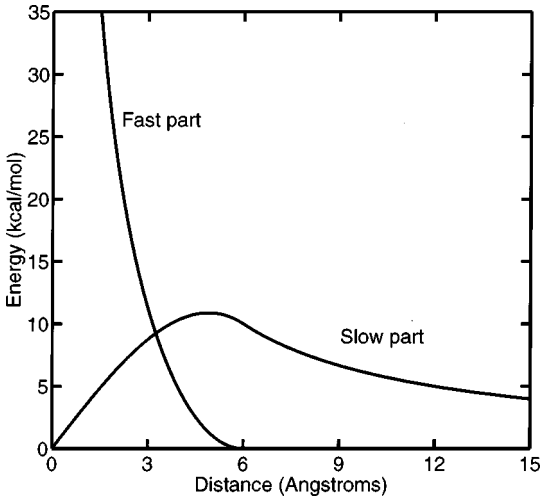

FIG. 1. Splitting of electrostatic potential into slow and fast parts. The electrostatic force is the derivative of this potential.

It turns out that in MD the systems integrated are chaotic. That is, very small perturbations to the initial conditions grow exponentially in time. Hence, it is inappropriate to expect that accurate trajectories for macromolecules be computed for more than a short time interval. Rather, it is expected only that the trajectories have the *correct statistical properties*. This is believed to be accomplished if the numerical integrator is symplectic, because the use of a symplectic integrator ensures that the system actually integrated by the numerical method is a slightly different Hamiltonian system.[13] On the other hand violations of this property such as that produced by velocity rescaling lead to skewed energy distributions.[14]

Reversibility is another important property of Eq. (5) that the numerical integrator should preserve. It has been stated[15] that ''any lack of perfection of such reversal should be due to rounding-off errors only, not the program.'' Many symplectic integrators are reversible. Reversibility and symplecticness (actually only volume preservation in phase space) are also sufficient for the validity of hybrid Monte Carlo methods, which employ short MD integrations.[16]

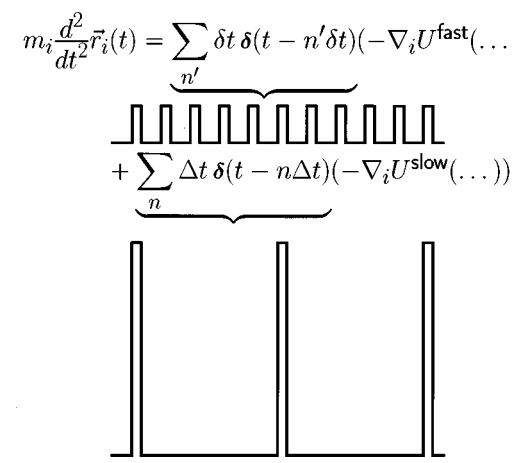

FIG. 2. Diagram for the multiple time-stepping impulse method.

The mollified impulse method that we describe in this paper is both symplectic and reversible, as we discuss in Sec. II.

C. MTS stability barriers

Based on accuracy considerations only, it seems that a largest Δt of 16 fs for the slowest forces should be achievable.[17] Considering that for large systems the bulk of the computational cost is in evaluating these slowest forces, this would represent substantial speedups over evaluating every 1 fs.

Nevertheless, if the frequency of the slow force impulse term on Eq. (6) coincides with a natural frequency of the system, then there may exist an oscillation in the positions whose amplitude increases with time (*resonance*). When resonance occurs, there is an accuracy reduction in the computation, and it may also lead to instability. The fastest normal modes of the system are the first to induce a resonance as Δt increases. Flexible covalent bonds to hydrogen in a biomolecule are usually responsible for the fastest normal modes, because among all interactions, bond stretchings have the largest force constants and hydrogen atoms have the smallest mass. The period of these modes is between 9 and 10 fs in molecules (cf. Sec. IV B).

Experiments[18] have shown that there is an upper limit of 4 fs (a 5 fs ''barrier'') in the longest time step Δt for the Verlet-I/r-RESPA method (*Impulse*). This barrier corresponds to a time step a bit smaller than half the period of the fastest normal mode, as is explained in Ref. 19. This barrier shifts upwards if the highest frequencies are eliminated by imposing constraints.

Instability problems are less severe for a biomolecule in an implicit solvent modeled by Langevin dynamics. There, the method termed LN[20] realizes the full potential of multiple time stepping.

D. Overcoming MTS stability barriers

In Sec. II we describe a symplectic and reversible modification to the impulse method, the mollified impulse method (MOLLY), and results obtained by applying the method to flexible water. MOLLY softens the contributions of the slow force impulse to bonded forces. Experience with Verlet-I/r-RESPA shows that flexible water is much more sensitive to instability than biomolecules.[21] Hence, we are confident that equally good behavior will occur for more heterogeneous simulations. Implementation requires only a little more than the programming of a SHAKE routine for constraining covalent bonds to hydrogens.[22]

The idea of the mollified impulse method is that one modifies the slow part of the potential energy U^{slow} so that it is evaluated at ''time averaged'' values of the positions, and one uses the gradient of this modified potential for the slow part of the force. The averaging is based on the effects of the ''fastest'' forces. Its net effect is to filter excitations of the slow impulses to the fastest motions which induce instability. This is described in Sec. II.

Averagings based in approximating the fastest forces by *B*-spline functions are described in Sec. II A. These methods allow increasing the time step to 5 fs, and therefore break the 5 fs time step barrier of the impulse method.

The main contribution of this paper is the *Equilibrium* version of the mollified impulse method, in which the averaging is defined to be a projection in configuration space onto the manifold defined by equilibrium positions for the fastest forces. With *Equilibrium*, it is possible to take time steps of 6 fs, a 50% acceleration over the *Impulse* method. It can be shown that, *for linear systems, Equilibrium's* long time step is not restricted by the frequency of the fastest force unlike *Impulse* and B-spline averaging MOLLY. *Equilibrium* is described conceptually in Sec. II B and algorithmically in the Appendix.

Experiments with all these methods are described in Sec. III. Also, progress has been made in understanding the limitations of the mollified impulse method. By contrived experiments, we have discovered that not only the fastest (bonded) forces but the fast parts of the nonbonded forces as well ($U_x^{\text{fast,nonbnd}}$) influence the stability of *Equilibrium* (see Sec. IV). We are developing a mollified method that will include $U_x^{\text{fast,nonbnd}}$ in the averaging to make even longer time steps possible.

II. MOLLIFIED IMPULSE METHOD (MOLLY)

This method, introduced in Refs. 4 and 19, is an attempt to evaluate the dynamics of the system more accurately and also to shift upwards the stability barriers on the time step by filtering excitations to the highest frequency forces. This is accomplished by a change to the impulse method

$$U^{\text{slow}}(x) \rightarrow U^{\text{slow}}(\mathcal{A}(x)), \tag{7}$$

which induces the change

$$F^{\text{slow}}(x) \rightarrow \mathcal{A}_x(x)^T F^{\text{slow}}(\mathcal{A}(x)). \tag{8}$$

This has two effects:

(1) *The force is evaluated at averaged positions*: This gives a more accurate description of the rapidly varying trajectory $X(t)$.

(2) The *destabilizing components of the* F^{slow} *impulse are removed*: the impulse is mollified. This transformation brings accuracy and stability gains.

One step of the mollified method (MOLLY) described above is

half a mollified kick

$$P^{n-1+\epsilon} = P^{n-1} + \frac{\Delta t}{2} F^{\text{slow},n-1}. \tag{9}$$

a vibration Propagate X^{n-1}, $P^{n-1+\epsilon}$ by integrating

$$\frac{d}{dt}X = M^{-1}P, \frac{d}{dt}P = F^{\text{fast}}(X), \tag{10}$$

(e.g., using Verlet/leapfrog with time step δt) for an interval Δt to get X^n, $P^{n-\epsilon}$.

a time averaging Calculate a temporary vector of time-averaged positions $\overline{X^n} = \mathcal{A}(X^n)$ and a Jacobian matrix $J^n = \mathcal{A}_x(X^n)^T$. The time-averaging function $\mathcal{A}(x)$ uses

only the fastest forces $F^{\text{fastest}}(x)$, to avoid the introduction of many nonzero elements into the Jacobian matrix.

half a mollified kick

$$F^{\text{slow},n} = J^n F^{\text{slow}}(\overline{X}^n), \tag{11}$$

$$P^n = P^{n-\epsilon} + \frac{\Delta t}{2} F^{\text{slow},n}. \tag{12}$$

The symbols $P^{n-1+\epsilon}$ and $P^{n-\epsilon}$ represent momenta just after the $(n-1)$st kick, and just before the nth kick, respectively. Note that $\overline{X}^n$ is used only for the purpose of evaluating F^{slow}; it does not replace the value of X^n.

The use of molecular dynamics as a tool to sample other ensembles is common practice. Combinations of Verlet-I/r-RESPA with constant-temperature NVT and constant-temperature- and -pressure NpT ensembles are proposed in Ref. 23. It should be straightforward to do a substitution of $U^{\text{slow}}(\mathcal{A}(x))$ for $U^{\text{slow}}(x)$ in these methods.

Since MOLLY is simply the application of Verlet-I/r-RESPA to a slightly modified potential energy, the symplecticness and reversibility of MOLLY follow from the symplecticness and reversibility of Verlet-I/r-RESPA. The only property needed for the averaging function $\mathcal{A}(x)$ is that it depends only on positions and it does because zero velocities are used in its calculation. In what follows, we present two instances of averaging functions that have this property.

A. B-spline averaging methods

A family of averagings is defined in Ref. 19:

$$\mathcal{A}(x) = \frac{1}{\Delta t}\int_0^\infty \phi\left(\frac{t}{\Delta t}\right)\tilde{X}(t)\,\mathrm{d}t,$$

where $\phi(t/\Delta t)$ is a weight function that is nonzero on a finite interval, and $\tilde{X}(t)$ solves an *auxiliary* problem

$$M\frac{\mathrm{d}^2}{\mathrm{d}t^2}\tilde{X} = F^{\text{fastest}}(\tilde{X}), \quad \tilde{X}(0) = x, \quad \frac{\mathrm{d}}{\mathrm{d}t}\tilde{X}(0) = 0. \tag{13}$$

We also need to compute $\mathcal{A}_x(x)^{\mathrm{T}}$. Weight functions defined by *B*-splines were used in Refs. 5 and 19. We implemented and tested several of those for this paper, plus a higher order one, *long quadratic average.* These weight functions are shown in Fig. 3, and their formulas are here:

long average

$\phi(s)=1, \quad |s|<1; \quad \phi(s)=\frac{1}{2}, \quad |s|=1;$

$\phi(s)=0, \quad |s|>1.$

long linear average

$\phi(s)=1-\frac{1}{2}s, \quad 0\leqslant s\leqslant 2; \quad \phi(s)=0, \quad |s|\geqslant 2.$

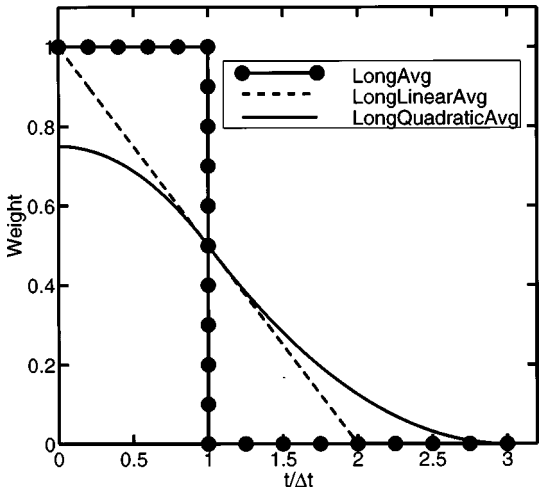

FIG. 3. Weight vs $t/\Delta t$ for first three B-spline filters.

long quadratic average

$\phi(s)=\frac{1}{4}(3-s^2), \quad |s|<1;$

$\phi(s)=\frac{1}{8}(3-s)^2, \quad 1\leqslant s\leqslant 3; \quad \phi(s)=0, \quad s\geqslant 3.$

Regarding the accuracy of these averaging methods, the original motivation behind them was to define $\mathcal{A}(x)$ in such a way that it compensated for the finite Δt of the Verlet-I/r-RESPA integrator. The positions $\mathcal{A}(x)$ are a function of Δt and

$$\mathcal{A}(x) = x + O(\Delta t^2),$$

so the error due to the modification of the potential is attributable to a finite time step Δt. Mathematical analysis and numerical experiments in Ref. 19 confirm that the trajectory error on a given time interval is proportional to Δt^2 independently of the stiffness of the fast modes for these B-spline averaging methods; this is not true for the Verlet-I/r-RESPA method. We do not discuss these averagings in further detail here because the experiments indicate that they are inferior to the *Equilibrium* method.

B. Equilibrium method

The mollified methods described above filter the slow force impulse in a partial way: their level of effectiveness is directly related to the extensiveness of their time averaging. Here, we introduce an averaging that completely eliminates the contributions of the slow force in the directions that excite the fastest forces in the system; that is, the bond and angle interactions. We project x onto the manifold in configuration space (the space of position coordinates) defined by the reference values of the bond lengths and bond angles.

The main assumption for the effectiveness of this method is that bond and angle interactions are the fastest forces and impose the most stringent requirement on the time step of *Equilibrium*. In cases where forces other than the fastest may induce instability, *Equilibrium* can be combined with other averagings.

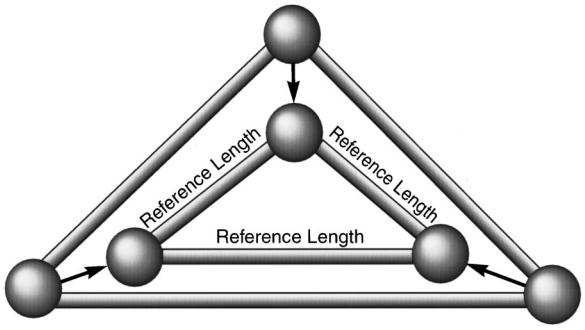

FIG. 4. Effect of *Equilibrium* on a water molecule. Atoms in the molecule are pulled toward their rest length position for the mollification (or filtering) of the slow force impulse, but left unchanged for the dynamics.

This averaging is obtained by determining the magnitude of the displacements along the bonds that would restore the bond lengths (and angles) to their reference value, and it is defined by

$$\mathcal{A}(x)=x+M^{-1}g_x(x)^{\mathrm{T}}\lambda, \tag{14}$$

with λ determined by the constraint equations

$$g(\mathcal{A}(x))=0. \tag{15}$$

This is similar to the constraining procedure used in SHAKE.[22] We provide algorithmic details in the Appendix. In fact, the calculation of $\mathcal{A}(x)$ is exactly SHAKE with zero velocities. *Equilibrium* MOLLY is not SHAKE, however, because $\mathcal{A}(x)$ is used only in the evaluation of F^{slow} and does not replace x in the integration. That is, we still use unconstrained dynamics. Figure 4 illustrates the effect of *Equilibrium* in a water molecule. Atoms in the molecule are pulled toward their rest length position for the mollification of the slow force impulse.

Regarding the accuracy of *Equilibrium*, unlike the B-spline averaging methods, there is no dependence of $\mathcal{A}(x)$ on Δt; rather, we would simply be advised to choose $\mathcal{A}(x)=x$ if Δt is small enough.

Here, we present the main motivation concerning the stability of this method by means of an example. Consider a system of two charged particles of unit mass interacting through a harmonic force (spring with reference length l), and a third, negatively charged, unit mass particle interacting through an electrostatic Coulomb force. This system has Hamiltonian

$$U=\tfrac{1}{2}k(x_1-x_2-l)^2-(x_3-x_2)^{-1}+(x_3-x_1)^{-1},$$

where $x_1<x_2<x_3$. Split the forces as $U_x^{\mathrm{fast}}(x)+U_x^{\mathrm{slow}}(x)$, with

$$U_x^{\mathrm{fast}}(x)=\begin{bmatrix} k(x_1-x_2-l) \\ -k(x_1-x_2-l) \\ 0 \end{bmatrix},$$

$$U_x^{\mathrm{slow}}(x)=\begin{bmatrix} -(x_3-x_1)^{-2} \\ (x_3-x_2)^{-2} \\ (x_3-x_1)^{-2}-(x_3-x_2)^{-2} \end{bmatrix}.$$

The [unmollified] slow force impulse changes the vibrational energy of the spring since the force on each atom is different. That is, the impulse stretches the spring. Both stretching modes are excited by the impulse. In contrast, the mollified impulse does not stretch the spring. The *Equilibrium* averaging

$$\mathcal{A}(x)=\begin{bmatrix} \frac{1}{2}(x_1+x_2)-\frac{1}{2}l \\ \frac{1}{2}(x_1+x_2)+\frac{1}{2}l \\ x_3 \end{bmatrix}, \quad \mathcal{A}_x(x)^{\mathrm{T}}=\begin{bmatrix} \frac{1}{2} & \frac{1}{2} & 0 \\ \frac{1}{2} & \frac{1}{2} & 0 \\ 0 & 0 & 1 \end{bmatrix},$$

eliminates this stretching effect by adding equal forces to each atom. The net effect of the mollified impulse is to translate the spring without any stretching. However, in 3D, these fastest forces are nonlinear. A mollified impulse will excite even those fastest forces for which the mollification is designed. Consider an impulse delivered at right angles to one of two balls connected by a spring. The impulse will act to stretch the spring.

III. EVALUATION OF METHODS

In this section, we present results of a comparison of various B-spline averaging methods, the *Equilibrium* mollified impulse method, the *Impulse* method, and constrained dynamics in combination with MTS (SHAKE-I). We show that the mollified methods shift the stability barrier on the time step upwards but do not eliminate it completely. *Impulse* is stable up to 4 fs, *B*-spline averaging MOLLY up to 5 fs, *Equilibrium* up to 6 fs, and SHAKE-I up to 8 fs. Even though SHAKE is the most stable method overall, it gives less accurate results, as the computation of radial distribution functions illustrates, whereas *Equilibrium's* is practically indistinguishable from Leapfrog. All these methods were tested in the molecular dynamics program NAMD.[24]

A. Test problem

We performed our simulations using flexible water, based upon the TIP3P model,[25] with flexibility incorporated by adding bond stretching and angle bending harmonic terms (cf. Ref. 6). We used a small problem consisting of a 10 Å radius sphere with 423 atoms equilibrated during 100 ps of simulation time by temperature rescaling to 300, 370, and 380 K. We also used a bigger problem consisting of a 20 Å radius sphere (3243 atoms), equilibrated to 340 K.

The potential energy of flexible water is given by

$$U^{\mathrm{electrostatic}}=C\frac{q_iq_j}{x_{ij}},$$

$$U^{\mathrm{Lennard\text{-}Jones}}=4\epsilon_{ij}\left(\left(\frac{\sigma_{ij}}{x_{ij}}\right)^{12}-\left(\frac{\sigma_{ij}}{x_{ij}}\right)^{6}\right)\mathrm{SW}(x_{ij}),$$

$$U^{\text{bond}} = K_B(x_{ij} - l_{ij})^2,$$

$$U^{\text{angle}} = K_A(\theta - \theta_0)^2,$$

where $x_{ij} = \|\vec{\mathbf{x}}_j - \vec{\mathbf{x}}_i\|$. For this discussion, these potentials are split as follows:

$$U^{\text{fast}} = U^{\text{fast,bnd}} + U^{\text{fast,nonbnd}},$$

$$U^{\text{fast,bnd}} = U^{\text{angle}} + U^{\text{bond}},$$

$$U^{\text{fast,nonbnd}} = U^{\text{fast,elect}} + U^{\text{Lennard-Jones}},$$

$$U^{\text{fast,elect}} = U^{\text{electrostatic}}\text{SW}(x_{ij}),$$

$$U^{\text{slow}} = U^{\text{electrostatic}} - U^{\text{fast,elect}}.$$

The switching function $\text{SW}(x_{ij})$ serves to split the electrostatic potential into slow and fast parts (and also to bring the Lennard-Jones force to zero smoothly) so that the force is a derivative of the potential even when using cutoff. It is defined by

$$\text{SW}(x_{ij}) = \begin{cases} 0 & \text{if} \quad x_{ij} > \text{cutoff}, \\ 1 & \text{if} \quad x_{ij} \leqslant \text{SW}_{\text{on}}, \\ \dfrac{(\text{cutoff}^2 - x_{ij}^2)(\text{cutoff}^2 + 2x_{ij}^2 - 3\text{SW}_{\text{on}}{}^2)}{(\text{cutoff}^2 - \text{SW}_{\text{on}}{}^2)} & \\ & \text{if} \quad \text{SW}_{\text{on}} \leqslant x_{ij} < \text{cutoff}. \end{cases}$$

For flexible water, $C = 332.0636\,(\text{kcal/mol})\text{K}^{-1}$, $K_A = 55\,(\text{kcal/mol})\text{degrees}^2$, $K_B = 450\,(\text{kcal/mol})\,\text{Å}^2$, $q_O = 0.417\,e$, $q_H = -0.834\,e$, $l_{O-H} = 0.957\,\text{Å}$, $l_{H-H} = 1.514\,\text{Å}$, $\theta_0 = 104.52$ degrees. The Lennard-Jones parameters are $\sigma_{H-H} = 0.4\,\text{Å}$, $\sigma_{O-H} = 1.75253\,\text{Å}$, $\epsilon_{H-H} = 0.046\,\text{kcal/mol}$, $\epsilon_{O-H} = 0.08365\,\text{kcal/mol}$. As indicated above, the system was equilibrated to 300, 340, 370, and 380 K.

B. Performance metrics

1. Energy conservation

For each simulation, we generated a history of all of the components of the energy, positions (trajectories), velocities, and forces. Most simulations ran for 200 ps, and several for 750 ps. These lengths allowed us to observe instabilities that were not evident in the first few picoseconds of simulation, and gave us significant confidence in our error estimates for energy conservation.

We monitored stability using the *pseudoenergy*. This quantity is the energy with $U^{\text{slow}}(x)$ replaced by $U^{\text{slow}}(\mathcal{A}(x))$. It is the quantity that the integrator is trying to conserve, and therefore is a better indicator of instability than the energy. The amount of fluctuation exhibited by the *pseudoenergy* is a fraction of the true energy's.

To measure drift in the energy, we devised a metric, the percent relative drift, given by $D = d/K$ where d is the absolute *pseudoenergy* drift (linear regression coefficient), and K is the average kinetic energy for the simulation.

Our experiments showed that D is a robust metric of drift and corresponds to our visual perception of the drift experienced by the methods we tested. The linear model applies to systems of interest where there is only slight growth. For severe instability, an exponential fit would be more adequate. We also computed the percent relative *noise* associated to the relative drift. It is the rms variation of the residual of the linear regression, and gives us an error bar of the drift for a given simulation length (cf. Refs. 18 and 26).

To measure accuracy, we computed a relative variation in the true energy, ΔE, given by

$$\Delta E = \frac{1}{KJ}\sum_{i=1}^{J} |e(i) - \overline{e}|,$$

where $\overline{e}$ is average total energy, $e(i)$ is instantaneous total energy, and J is simulation length (in time steps). For symplectic integrators, ΔE is an excellent indicator of accuracy: it measures the distance between the true energy surface in phase space and a modified energy surface arising from the use of a finite time step Δt (see Ref. 13, p. 132). The difference between the two energy surfaces will determine the accuracy with which most quantities are calculated.

2. Statistical quantities

We computed structural and dynamical properties for the various integrators. We obtained radial distribution functions of the test problem for site–site O–O, O–H, and H–H interactions for the flexible TIP3P water (cf. Ref. 25). These were computed using XPLOR's trajectory analysis capabilities. We also obtained the mean square displacement $R(\tau)$ (MSD) as a function of time and the self-diffusion coefficient D using Einstein's relation $3D = R(\tau)/(2\tau)$. The procedure to compute these quantities is described in more detail in Refs. 6 and 27, among others. The self-diffusion coefficient was computed by averaging over all molecules and all time origins of 100 ps simulations of a 10 Å radius sphere of water (141 molecules). To get the diffusion coefficient for liquid water, one would normally use periodic boundary conditions to avoid surface tension effects. The program NAMD 1.5 in which we have tested our methods does not implement periodic boundary conditions with an Ewald sum (although it is implemented in NAMD 2.0[28]). Hence, we have used spherical constraints with a radius of 11 Å and 21 Å (to reduce surface effects) and averaged the results. There was no discernible difference in quality between the two sets of results. The quantities we compute are not physically correct but they are of the same nature as the physical quantities and should serve well to compare the proposed methods to the Leapfrog method, which is of known quality.

C. Results

Here, we summarize the results of our experiments. Figure 5 compares the stability of *Impulse, Equilibrium*, and SHAKE-I (SHAKE using *Impulse* MTS as the integrator). As mentioned above, SHAKE-I is the most stable of all the methods, for time steps up to 8 fs; *Impulse* is stable up to 4 fs; *Equilibrium* is stable up to 6.25 fs. Figure 6 shows their relative accuracy. Observe that the inaccuracies with long time steps are mostly due to the drift in the energy. Both of the above figures plot the results for simulations of water at 300 K for Δt up to 7 fs, and at 380 K for Δt of 8 fs or more.

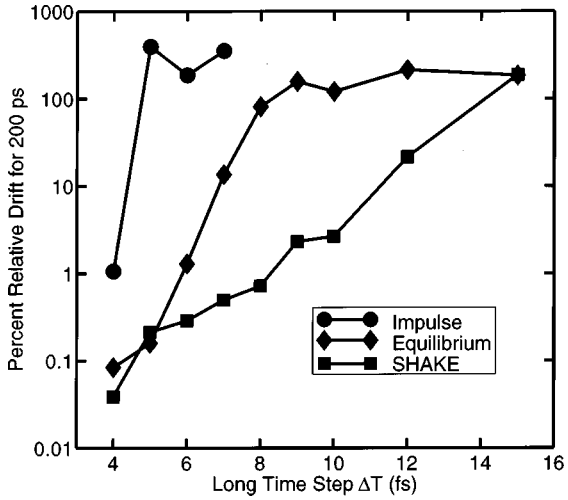

FIG. 5. Percent relative drift D (kcal mol^{-1}K^{-1}) for 200 ps vs Δt (fs).

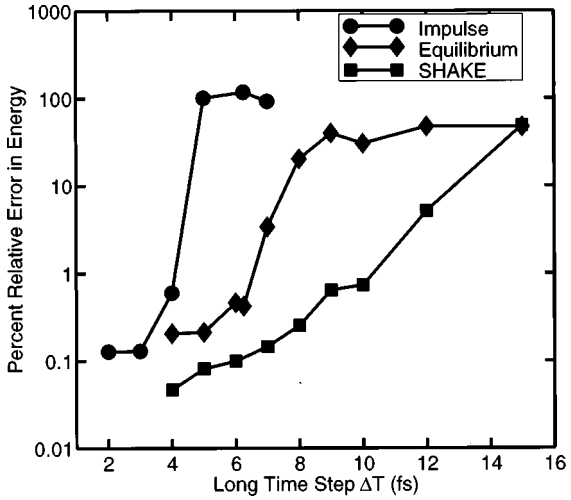

FIG. 6. Percent relative variation in energy ΔE (kcal mol^{-1} K^{-1}) vs Δt (fs).

Tables I and II list results of 200 ps simulations of 125 waters for *Impulse, Equilibrium,* and SHAKE-I at 300 and 380 K respectively. They are sorted by Δt, the method, and δt for easy comparison among methods for a given long time step Δt. Similarly, Table III lists results of 750 ps simulations. All the experiments with 125 waters use a cutoff of 6.5 Å for Lennard-Jones and short-range electrostatic force computation. This is shorter than usual for testing purposes — with a more customary cutoff of 8 Å or greater, the long-range force would be too weak to test the integrators due to the small number of atoms. Other parameters are SW_{on} (dis-

TABLE I. Results for 200 ps of simulation of flexible water at 300 K. All experiments use spherical boundary conditions with a radius of 21 Å, except those marked with ''*,'' which do not use spherical BCs. The drift and noise are the coefficient and rms variation on the residual, respectively, of a linear regression on the energy.

Δt (fs)	Method	δt (fs)	SW_{on} (Å)	Drift	Noise (kcal mol^{-1}K^{-1})	ΔE
0.5	Leapfrog	0.5	4	−0.009%	0.290%	0.029%
1	Leapfrog	1	4	0.028%	0.280%	0.122%
2	Impulse	1	4	−0.019%	0.220%	0.128%
3	Impulse	1	4	0.087%	0.170%	0.130%
4	Equilibrium	1	4	0.084%	0.160%	0.206%
4	Impulse	1	4	1.060%	0.190%	0.305%
4	SHAKE-I	1	4	0.039%	0.310%	0.047%
5	Equilibrium	1	4	0.159%	0.170%	0.213%
5	Impulse	1	4	396.000%	8.800%	101.000%
5	SHAKE-I	1	2	−0.043%	0.130%	0.045%
5	SHAKE-I	1	4	0.214%	0.083%	0.082%
6	Equilibrium	0.5	2	0.575%	0.110%	0.202%
6	Equilibrium	0.5	4	1.040%	0.160%	0.317%
6	Equilibrium*	1	2	1.590%	0.210%	0.417%
6	Equilibrium	1	2	1.960%	0.220%	0.557%
6	Equilibrium*	1	4	1.290%	0.260%	0.382%
6	Equilibrium	1	4	1.380%	0.260%	0.422%
6	Impulse	1	4	187.000%	8.400%	47.200%
6	SHAKE-I	1	2	0.086%	0.370%	0.052%
6	SHAKE-I	1	4	0.288%	0.140%	0.099%
6.25	Equilibrium	0.625	2	1.630%	0.190%	0.423%
6.25	Equilibrium*	1.25	2	2.270%	0.350%	0.622%
6.25	Impulse	0.625	2	456.000%	11.000%	118.000%
6.25	SHAKE-I	0.625	2	0.020%	0.390%	0.047%
7	Equilibrium*	1	2	13.600%	0.280%	3.410%
7	Equilibrium	1	4	17.700%	0.830%	4.590%
7	Impulse*	1	2	355.000%	33.000%	92.800%
7	SHAKE-I	1	4	0.498%	0.100%	0.146%
8	Equilibrium	1	2	57.900%	1.010%	14.600%
8	Equilibrium	1	4	86.100%	2.687%	22.100%
9	SHAKE-I	1	4	2.465%	0.230%	0.630%

TABLE II. Results for 200 ps of simulation of flexible water at 380 K. All experiments use spherical boundary conditions with a radius of 41 Å, except those marked with ''*,'' which do not use spherical BCs. SW_{on} is 4. The drift and noise are the coefficient and rms variation on the residual, respectively, of a linear regression on the energy.

Δt (fs)	Method	δt (fs)	Drift	Noise (kcal mol^{-1}K^{-1})	ΔE
6.25	Equilibrium	0.625	4.050%	0.200%	1.060%
6.25	Equilibrium	1.25	15.560%	0.470%	2.000%
6.25	SHAKE-I	0.625	0.232%	0.280%	0.054%
7	Equilibrium*	0.5	10.860%	0.300%	1.440%
7	SHAKE-I	1	-0.025%	0.080%	0.064%
8	Equilibrium	1	81.300%	1.500%	20.300%
8	SHAKE-I	1	0.720%	0.310%	0.253%
9	Equilibrium	1	158.000%	2.200%	40.000%
9	SHAKE-I	1	2.310%	0.350%	0.642%
10	Equilibrium	1	121.000%	2.400%	30.500%
10	SHAKE-I	1	2.660%	0.400%	0.733%
12	Equilibrium	1	214.444%	5.100%	47.800%
12	SHAKE-I	1	21.600%	0.910%	5.150%
15	Equilibrium	1	185.000%	25.000%	47.300%
15	SHAKE-I	1	188.000%	11.000%	48.900%

tance at which a C^2 switching function is activated) and the small time step δt. Notice that a smaller δt reduces the drift observed in a simulation. For example, *Equilibrium* with $\Delta t = 6$ fs and $SW_{on} = 2$ Å, has a drift of 1.96% in 200 ps with $\delta t = 1$ fs, and only 0.575% in 200 ps with $\delta t = 0.5$ fs. A similar trend is observed in the rest of these tables.

We have evidence that a sufficiently nonsmooth switching function creates extreme instability. For example, in a test of a protein and water (15 000 atoms) at 300 K using the *Impulse* method with a Δt of 4 fs, we get no drift using the C^2 switching function implemented in NAMD and described in Ref. 18. However, using the XPLOR switching function[29] for the same problem and parameters above gives a drift of 44 000% per ns!

Figures 7–9 show the radial distribution functions for the site-to-site O–O, O–H, and H–H interactions for *Equilibrium* with $\Delta t = 6$ fs, $\delta t = 1$ fs; Verlet/leapfrog with $\delta t = 1$ fs; and SHAKE-I. Notice the close agreement between the methods using unconstrained dynamics, and the shift in phase exhibited by SHAKE-I. This shift is more pronounced in the O–O and O–H radial distributions but is nevertheless noticeable in the H–H distribution function. It is important to note that this is not only an effect of the large time step used (8 fs) for SHAKE-I. The same shift is observed with smaller time steps. This is expected, since SHAKE-I eliminates several degrees of freedom from the dynamics. These radial distribution functions were obtained by sampling simulations of 100 ps.

Table IV lists the self-diffusion coefficient and the standard deviation computed using the above methodology. The uncertainty in the computation grows slightly for *Impulse* and *Equilibrium* as Δt increases. However, no statistically significant difference can be detected for either method and parameters. The inaccuracy in the computation for SHAKE-I grows more pronouncedly with $\Delta t = 8$ fs, but it remains the

TABLE III. Results for 750 ps of simulation for water. Most experiments are at 300 K. Those marked with a ''+'' are at 380 K. All experiments use spherical boundary conditions with a radius of 21 Å, except those marked with ''*,'' which do not use spherical BCs. The drift and noise are the coefficient and rms variation on the residual, respectively, of a linear regression on the energy.

Δt (fs)	Method	δt (fs)	SW_{on} (Å)	Drift	Noise (kcal mol^{-1}K^{-1})	ΔE
1	Leapfrog	1	4	0.258%	0.340%	0.125%
4	Impulse	1	4	2.000%	0.500%	0.598%
5	Impulse	1	4	1320.000%	18.000%	327.000%
5	SHAKE-I	1	2	−0.030%	0.440%	0.047%
6	Equilibrium	1	2	6.120%	0.420%	1.580%
6	Equilibrium	1	4	2.050%	0.340%	0.461%
6	SHAKE-I	1	2	0.131%	0.250%	0.063%
6.25	Equilibrium+	0.625	4	14.880%	0.440%	2.620%
6.25	Equilibrium	0.625	2	8.795%	0.330%	1.430%
6.25	Equilibrium+	1.25	4	34.350%	1.000%	5.680%
6.25	Equilibrium*	1.25	2	15.112%	0.640%	4.820%
6.25	SHAKE-I	0.625	2	0.118%	0.340%	0.048%
7	Equilibrium	1	4	53.788%	1.100%	10.600%

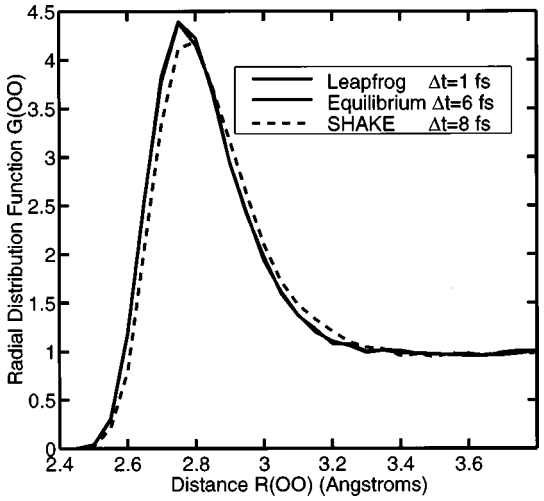

FIG. 7. Radial distribution function for the O–O interaction for three different integrators. Notice that *Equilibrium*'s is indistinguishable from Leapfrog, but SHAKE's peak is in a different position.

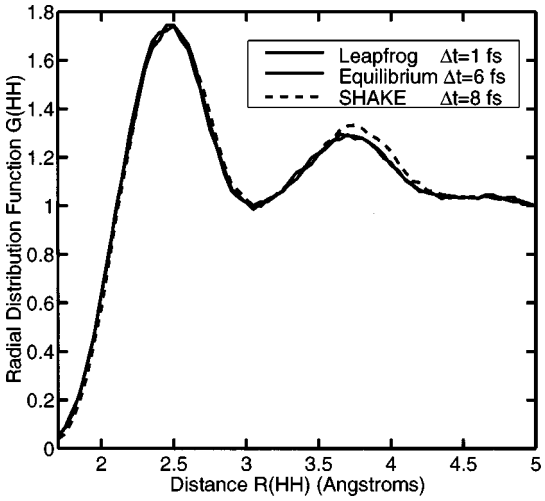

FIG. 9. Radial distribution function for the H–H interaction for three different integrators. Notice that *Equilibrium*'s is indistinguishable from Leapfrog, but SHAKE's peak is slightly shifted and higher.

same at $\Delta t = 6$ fs. We comment next on each method separately.

D. *Equilibrium* MOLLY

We implemented *Equilibrium* into NAMD (http://www.ks.uiuc.edu/Research/namd/namd/html) version 1.5, using the algorithm given in the Appendix. We validated and tested this method extensively. It has been shown to be stable for Δt of up to 6 or 6.25 fs. Our standard for comparison is the *Impulse* method with $\Delta t = 4$ fs, $\delta t = 1$ fs, which according to Table I has a drift of 1.06% for 200 ps. Fig. 10 shows that *Equilibrium* at 6.25 is superior to an averaging method and to the *Impulse* method. The value $\Delta t = 6.25$ fs is particularly useful, since it divides evenly into 100 and is machine representable.

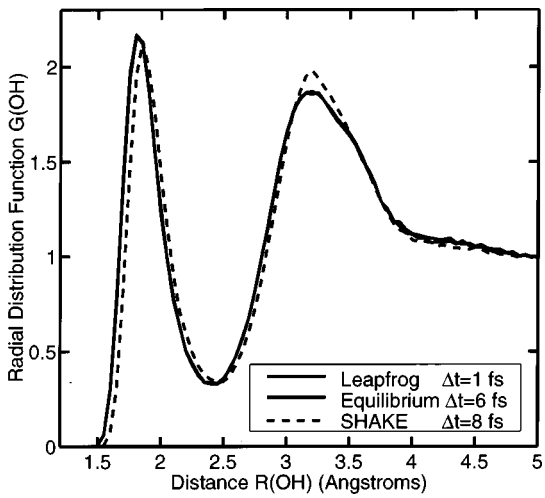

FIG. 8. Radial distribution function for the O–H interaction for three different integrators. Notice that *Equilibrium*'s is indistinguishable from Leapfrog, but SHAKE's peak is in a different position.

E. SHAKE-I: SHAKE plus the *Impulse* method

We tested SHAKE as implemented in NAMD 1.5 using the MTS *Impulse* method as the integrator (SHAKE-I). This approach is a more radical treatment of the bond and angle forces than *Equilibrium*, because it eliminates their contribution to the dynamics altogether. These experiments were a valuable test of the viability of constrained dynamics and MTS methods.

They also served to corroborate that the bond and angle forces are responsible for instabilities. The numerical experiments showed that SHAKE-I is stable for Δt of up to 8 fs but is slightly unstable for time steps Δt of 9 fs.

These results suggest that the bond and angle forces are partly responsible for the instabilities observed in the methods discussed in this paper. Further analysis (described in Sec. IV) leads us to conclude that the contributions of the Lennard-Jones interactions to the ''bond-stretching'' normal modes are also important. Hence, the averaging including the fastest forces only is not enough to get rid of all instabilities, since their source should be traced not only to the fastest (bonded) forces but to the fast part of at least some nonbonded forces as well.

F. Averaging MOLLY

We also implemented the *long average*, *long linear average*, and *long quadratic average* methods described above. Our implementation used Hessian matrices (required for the

TABLE IV. Self-diffusion coefficient (10^{-5} cm^2/s). Values with standard deviations were computed by averaging over all molecules and all time origins of 100 ps simulations of a 10 Å radius sphere of water (141 molecules.)

	$\delta t, \Delta t$ (fs)					
Method	0.5	1	1,4	0.5,6	1,6	1,8
Impulse	8.9±0.3	8.9±0.3	9.0±0.4			
Equilibrium	9.4±0.4	9.1±0.3		9.2±0.4	9.3±0.4	
SHAKE-I	9.0±0.3	8.9±0.5		9.1±0.3		10.1±0.8

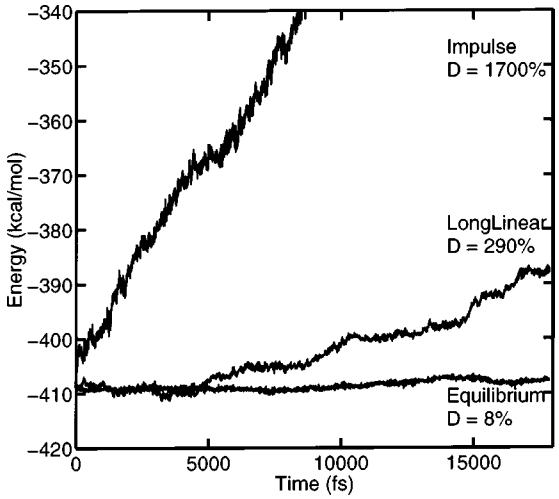

FIG. 10. Mollified methods with $\Delta t = 6.25$ fs.

mollification of the slow force impulse) generated by automatic differentiation tools for C++ developed at Argonne National Labs.[30] These experiments showed that all three averaging methods work for $\Delta t = 5$ fs, succeeding in breaking the 5 fs barrier of the impulse method. This is illustrated in Fig. 11. However, these averaging methods are less robust than *Equilibrium*.

Results (not given here) show that it makes little difference to include the angle forces; most of the benefit in stability comes from mollifying the bond forces. Hence, it is likely that a variation of *Equilibrium* that constrains only O–H bonds would be as good as one that also constrains angles (e.g., the H–H distances in water).

IV. EXPERIMENTAL STABILITY ANALYSIS

After observing instabilities for *Equilibrium* at 8 fs, we sought to discover which components of the force are responsible for the instability, in order to devise a stronger mollification for those components, or some other mechanism to correct instabilities. Because of noise, simple observation of the energy components does not reveal which one rises first.

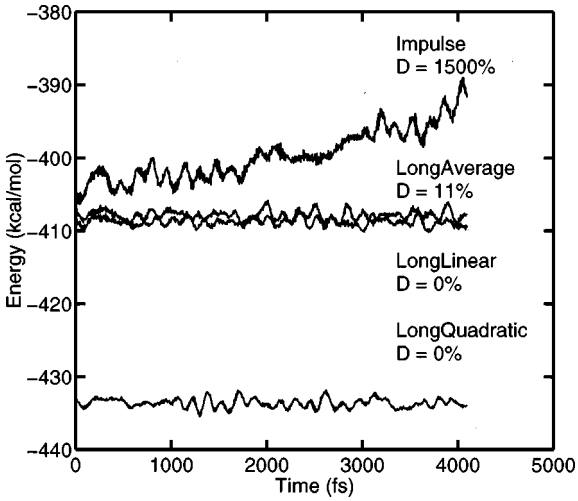

FIG. 11. Averaging methods at $\Delta t = 5$ fs.

A. First experiment

One study was an attempt to reduce nonlinear effects by doing an experimental small-energy analysis. This consists of running simulations with coordinates near a stable equilibrium of the Hamiltonian. For this, we ran simulations on the test problem with minimized energy (near zero Kelvin).

The reason for this analysis is twofold: First, by starting the simulation close to an equilibrium point, KAM (Kolmogorov–Arnol'd–Moser) theory[31] shows that the solution will remain close to the equilibrium at all times except for instabilities caused by resonances of time steps whose length is close to some multiple of 1/3, or 1/4, of some natural period in the system. This holds provided a non degeneracy condition is satisfied and Arnol'd diffusion can be neglected (cf. Ref. 32). Second, it avoids the strong coupling of normal modes that happens at higher temperatures allowing the more precise use of spectral analysis.

We ran simulations for 750 ps with flexible water near 0 K with Δt from 5 to 12 fs, every 0.1 fs. These experiments showed instabilities starting at $\Delta t = 7.7$ fs for the regular water. To check the validity of our assumption that the fastest forces (bond and angle) are responsible for these instabilities, we conducted a series of experiments with ''accelerated'' water at the same temperature.

The latter water model was designed to produce the destabilizing effects of the bond and angle force for smaller values of Δt (at $\Delta t^{\text{fast}} = 0.8\Delta t^{\text{regular}}$). It is a modification of the test problem already described, where the bond and angle force constants were multiplied by $(5/4)^2 = 25/16$. This is equivalent to multiplying the frequency by 5/4. The set of experiments with the fast water showed a similar pattern of instabilities as the regular water, but with slightly smaller drifts and strong instabilities appearing at $\Delta t^{\text{fast}} = 6.4$ fs (a ''scaled'' $\Delta t = 8$ fs), rather than 6.16 fs (a scaled $\Delta t = 7.7$ fs).

Figure 12 shows D vs Δt (scaled for the fast water). This suggests that there may be other force components causing instability besides the angle and bond forces. We then accelerated another force, the Lennard-Jones interaction. After doing this we got a much better scaling. The asterisks in Fig. 12 correspond to the water model with accelerated angle, bond, and Lennard-Jones interactions. Therefore, it would help to include the fast part of the Lennard-Jones force in the averaging (the frequency of the slowest parts of this force is very slow and unlikely to have any contribution to the stability of *Equilibrium*).

B. Normal mode analysis

Normal mode analysis was performed for the test problem in the manner described in Ref. 6. Equation (5) can be approximated linearly at an equilibrium $U_x(x_0) = 0$ by

$$M \frac{\mathrm{d}^2}{\mathrm{d}t^2} x = -U_x(x) = -U_{xx}(x_0)(x - x_0) - O(\|x - x_0\|^2).$$

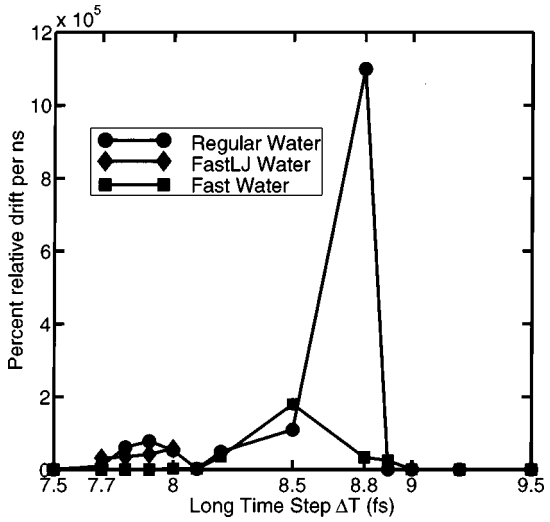

FIG. 12. Percent relative drift per ns (D) vs Δt for **regular**, **fast,** and **fast LJ** water.

Then, we can transform our problem into a set of harmonic oscillators

$$\frac{\mathrm{d}}{\mathrm{d}t}x_i = p_i, \quad \frac{\mathrm{d}}{\mathrm{d}t}p_i = -\omega_i^2 x_i,$$

$$\omega_i^2 = \lambda_i(M^{-1/2}U_{xx}M^{-1/2}),$$

whose solution is a superposition of oscillations (*normal modes*) with periods $\tau^{-1}=\omega_i/2\pi$ and with directions given by eigenvectors. For example, a linear triatomic molecule with 3 unit masses connected by 2 springs of stiffness k has a matrix $M^{-1/2}U_{xx}M^{-1/2}$ with

eigenelements

$$= \begin{cases} \lambda = k, & y = [1 \quad 0 \quad -1] & \text{symmetric stretch,} \\ \lambda = 0, & y = [1 \quad 1 \quad 1] & \text{translation,} \\ \lambda = 3k, & y = [\tfrac{1}{2} \quad -1 \quad \tfrac{1}{2}] & \text{asymmetric stretch.} \end{cases}$$

The matrix $\mathcal{A}_x(X^n)^{\mathrm{T}}$ for *Equilibrium* removes the stretching components. Periods of the normal modes for our test problem near 0 K are presented in Table V. The first column is the average period for similar normal modes from different molecules. The last two columns are the minimum and maximum value of the periods. The first two rows correspond to the bond stretchings, the next to the angle bending. In the absence of other forces, there would be no other frequencies. The last row shows the effect of the Lennard-Jones and electrostatic forces, with periods as fast as 38.235 fs and as slow as 2890.3 fs.

TABLE V. Period of the normal modes of 125 waters ranked from highest to lowest frequency. The first column is the average period for normal modes from all molecules. The last two columns give the minimum and maximum period. The first two rows are bond-stretching normal modes; the third is the angle bending normal mode. The last row shows normal modes produced by the Lennard-Jones and electrostatic forces.

Rank	Avg (fs)	Min (fs)	Max (fs)
1–125	9.898	9.821	9.976
126–250	10.083	9.978	10.197
251–375	18.844	18.232	19.440
376–1119		38.235	2890.3

C. Another experiment: Pure *Equilibrium*

This experiment was performed to show that the instabilities in *Equilibrium* stem from the effect of the fast nonbonded forces on the fastest forces, and therefore it is important to include the former in the averaging.

Pure *Equilibrium* is *Equilibrium* with all but the fastest forces included in the long-time step, that is, $F^{\mathrm{slow}} = F^{\mathrm{slow,elect}} + F^{\mathrm{fast,nonbnd}}$. For accuracy and stability, a much shorter long time step ($\Delta t = 2$) must be used. In order to test for instabilities the fastest forces were made faster by a factor of 4. The following results seem to indicate that *Pure Equilibrium* performs nearly as well as SHAKE-I. This means that the effects of the fast nonbonded forces are important for the stability of *Equilibrium.*

Method	Drift	Noise
Shake ($\Delta t = 2$)	0.04%	0.47%
Pure Equil ($\Delta t = 2$,scaled $\Delta t = 8$)	0.10%	0.85%
Equilibrium ($\Delta t = 8$)	57.90%	0.01%
Shake ($\Delta t = 8$)	0.70%	0.30%

These results are for 200 ps run for all of the above. At $\Delta t = 8$ $\mathrm{SW_{on}}$ is 2 Å. With $\mathrm{SW_{on}} = 4$ Å, *Equilibrium* does worse (86.1%±2.7%) and the results are more dramatic. The scaled $\Delta t = 8$ corresponds to multiplying the bond force constant by 16, a fourfold increase in the bond energy.

ACKNOWLEDGMENTS

We are grateful to Nick Dietz for doing some of the simulation runs, and helping in the implementation of the normal mode analysis. We are also thankful to Dr. Neal Krawetz, for assisting us in the implementation of *Equilibrium* into NAMD. Alexander Balaeff's help with producing the diffusion coefficient is much appreciated. Finally, Justin Wozniak helped produce the final versions of the figures. This work was supported in part by NIH Grant No. P41RR05969 and NSF Grants Nos. BIR-9318159, BIR-9423827 (EQ), and DMS-9600088.

APPENDIX: THE *Equilibrium* MOLLIFIED IMPULSE METHOD

In analogy to the procedure used by SHAKE to constrain bond lengths, we define the *Equilibrium* averaging $\mathcal{A}(x)$ to be

$$\mathcal{A}(x) = x + M^{-1}g_x(x)^T\lambda, \text{with } g(\mathcal{A}(x)) = 0. \tag{A1}$$

We are hereby computing displacements $M^{-1}g_x(x_0)^T\lambda$ that keep the bond lengths constant, thereby finding the ''equilibrium'' positions $\mathcal{A}(x)$ (if only the fastest forces are present).

From $g_x(\mathcal{A}(x))^T\mathcal{A}_x(x) = 0$, obtained by differentiating Eq. (A1), it follows that, by design, we are annihilating the components of the slow force in the directions spanned by the columns of $g_x(\mathcal{A}(x))$. These are the directions in configuration space along which the bond length and angle

forces can get excited and induce instability. The main assumption for the effectiveness of this method is that bond and angle interactions are the fastest forces, whose contributions influence stability the most. In cases where other forces may induce instability (for example, Lennard-Jones interactions), this method cannot be extended satisfactorily.

Our numerical simulations were on flexible water. For each water molecule there are three constraints of the form

$$g^{ij}(x)=\|\vec{\mathbf{x}}_j-\vec{\mathbf{x}}_i\|^2-l_{ij}^2, \tag{A2}$$

where l_{ij}^2 is the square of the reference bond length, $1\leqslant i<j\leqslant 3$. For general molecules, we constrain only the bonds to H. Notice that we can easily analytically compute $g_x(x)$ and $g_{xx}(x)$; for example,

$$g_x^{12}(x)=2\begin{bmatrix}\vec{\mathbf{x}}_i-\vec{\mathbf{x}}_j\\ \vec{\mathbf{x}}_j-\vec{\mathbf{x}}_i\\ 0\end{bmatrix},$$

$$g_{xx}^{12}=2\begin{bmatrix}I & -I & 0\\ -I & I & 0\\ 0 & 0 & 0\end{bmatrix}.$$

For each water molecule we have three λ^{ij} to determine by solving a system of three nonlinear equations $g(x+M^{-1}g_x(x)^{\mathrm{T}}\lambda)=0$. We iterate using Newton's method to solve for a function

$$\Psi(\lambda)\equiv g(\mathcal{A}(x))=0,$$

$$\text{with an iteration } \lambda^{+}=\lambda-\Psi_{\lambda}^{-1}(\lambda)\Psi(\lambda)$$

$$\text{where } \Psi_{\lambda}=g_x(\mathcal{A}(x))M^{-1}g_x(x)^{\mathrm{T}}.$$

In this way we determine λ and $\mathcal{A}(x)$.

Next, we compute $\mathcal{A}_x(x)$. Differentiating Eq. (A1) gives

$$\mathcal{A}_x(x)=I+M^{-1}\sum_{ij}\lambda^{ij}g_{xx}^{ij}(x)+M^{-1}g_x(x)^{\mathrm{T}}\lambda_x. \tag{A3}$$

At this point we need λ_x, which we get from substituting Eq. (A3) into Eq. (A1), yielding

$$\lambda_x=-(g_x(\mathcal{A}(x))M^{-1}g_x(x)^{\mathrm{T}})^{-1}g_x(\mathcal{A}(x))\times\left(I+M^{-1}\sum_{ij}\lambda^{ij}g_{xx}^{ij}\right). \tag{A4}$$

Using Eq. (A4), we rewrite Eq. (A3) as

$$\mathcal{A}_x(x)=(I-M^{-1}g_x^{\mathrm{T}}(\overline{g_x}M^{-1}g_x^{\mathrm{T}})^{-1}\overline{g_x})\times\left(I+M^{-1}\sum_{ij}\lambda^{ij}g_{xx}^{ij}\right), \tag{A5}$$

where $\overline{g_x}=g_x(\mathcal{A}(x))$, and $g_x=g_x(x)$. Equation (A5) is used to compute $\mathcal{A}_x(x)$ given $\mathcal{A}(x)$ and x.

[1] H. Grubmüller, Master's thesis, Physik-Dept. der Tech. Univ. München, Munich, 1989.
[2] H. Grubmüller, H. Heller, A. Windemuth, and K. Schulten, Mol. Simul. **6**, 121 (1991).
[3] M. Tuckerman, B. J. Berne, and G. J. Martyna, J. Chem. Phys. **97**, 1990 (1992).
[4] B. García-Archilla, J. M. Sanz-Serna, and R. D. Skeel, in *Numerical Analysis 1997*, edited by D. F. Griffiths and G. A. Watson (Pitman, London, 1998), pp. 111–123.
[5] R. D. Skeel and J. Izaguirre, in ''Computational Molecular Dynamics: Challenges, Methods, Ideas,'' Vol. 4 of *Lecture Notes in Computational Science and Engineering*, edited by P. Deuflhard *et al.* (Springer, Berlin, 1998), pp. 318–331.
[6] A. R. Leach, *Molecular Modelling: Principles and Applications* (Addison-Wesley Longman, Reading, MA, 1996).
[7] M. Saito, J. Chem. Phys. **101**, 4055 (1994).
[8] D. M. York, W. T. Yang, H. Lee, T. Darden, and L. G. Pedersen, J. Am. Chem. Soc. **117**, 5001 (1995).
[9] D. Kosztin, T. C. Bishop, and K. Schulten, Biophys. J. **73**, 557 (1997).
[10] P. Procacci and M. Marchi, J. Chem. Phys. **104**, 3003 (1996).
[11] P. Procacci, M. Marchi, and G. J. Martyna, J. Chem. Phys. **108**, 8799 (1998).
[12] S. O. Samuelson and G. J. Martyna, J. Chem. Phys. **109**, 11061 (1998).
[13] J. Sanz-Serna and M. Calvo, *Numerical Hamiltonian Problems* (Chapman and Hall, London, 1994).
[14] S. C. Harvey, R. K. Z. Tan, and T. E. Cheatham, J. Comput. Chem. **19**, 726 (1998).
[15] O. Buneman, J. Comput. Phys. **1**, 517 (1967).
[16] B. Mehlig, D. W. Heermann, and B. M. Forrest, Phys. Rev. B **45**, 679 (1992).
[17] T. Forester and W. Smith, Mol. Simul. **13**, 195 (1994).
[18] D. D. Humphreys, R. A. Friesner, and B. J. Berne, J. Phys. Chem. **98**, 6885 (1994).
[19] B. García-Archilla, J. M. Sanz-Serna, and R. D. Skeel, SIAM J. Sci. **20**, 930 (1998).
[20] E. Barth and T. Schlick, J. Chem. Phys. **109**, 1617 (1998).
[21] T. Bishop, R. D. Skeel, and K. Schulten, J. Comput. Chem. **18**, 1785 (1997).
[22] J. Ryckaert, G. Ciccotti, and H. Berendsen, J. Comput. Phys. **23**, 327 (1977).
[23] G. J. Martyna, M. E. Tuckerman, D. J. Tobias, and M. L. Klein, Mol. Phys. **87**, 1117 (1996).
[24] M. Nelson, W. Humphrey, A. Gursoy, A. Dalke, L. Kalé, R. Skeel, and K. Schulten, Int. J. Supercomput. Appl. **10**, 251 (1996).
[25] W. L. Jorgensen, J. Chandrasekhar, J. D. Madura, R. L. Impey, and M. L. Klein, J. Chem. Phys. **79**, 926 (1983).
[26] H. Ishida, Y. Nagai, and A. Kidera, Chem. Phys. Lett. **282**, 115 (1998).
[27] D. Okunbor and R. D. Skeel, J. Comput. Chem. **15**, 72 (1994).
[28] L. Kalé, R. Skeel, R. Brunner, M. Bhandarkar, A. Gursoy, N. Krawetz, J. Phillips, A. Shinozaki, K. Varadarajan, and K. Schulten, J. Comp. Phys. (1998) (in press).
[29] A. T. Brünger, X-PLOR, *Version 3.1: A System for X-ray Crystallography and NMR*, The Howard Hughes Medical Institute and Department of Molecular Biophysics and Biochemistry, Yale University, New Haven, CT, 1992.
[30] A. Griewank, D. Juedes, and J. Utke, ACM Trans. Math. Softw. **22**, 131 (1996).
[31] V. I. Arnol'd, *Mathematical Methods of Classical Mechanics*, 2nd ed. (Springer, New York, 1989).
[32] V. I. Arnol'd, *Geometrical Methods in the Theory of Ordinary Differential Equations* (Springer, New York, 1988).